Acta Neurochir (Wien) (1999) 141: 1025–1038

Acta Neurochirurgica

One Atlas – Three Anatomies: Relationships of the Schaltenbrand and Wahren Microscopic Data

K. Niemann and **I. van Nieuwenhofen**

Department of Neuroanatomy, University of Technology (RWTH), Aachen, Germany

Summary

The stereotaxic atlas of Schaltenbrand and Wahren is widely used for orientation in functional neurosurgery of the human diencephalon. As the sagittal, frontal, and horizontal microscopic series were gathered from three different cerebral hemispheres, loci with the same ACPC (anterior commissure–posterior commissure) coordinates are not exactly anatomically corresponding.

We compared the 3-D position of 21 anatomical structures in the three series based on their digitally interpolated solid volume representations. Regression analysis of the centres of gravity revealed strong linear correlations beween series ($0.944 \leq$ Pearson's $r \leq 0.976$, $\alpha < 0.0001$). Thus calculation of anatomically corresponding sites based on the regression equations seems justified. Volumetry revealed that the sagittally sectioned thalamus is $\approx 10\%$ larger than the frontally and 40% larger than the horizontally sectioned thalamus. So as to match it to the sagittal series, the frontal series has to be widened in lateral direction by 19%, in anteroposterior and dorsobasal (vertical) direction it has to be compressed by 5 and 9%, respectively. In contrast, the distance of structures from the midline in the horizontal and sagittal series is very similar. The horizontal series is, however, 25% smaller than the sagittal one in anteroposterior and 17% in vertical direction. On average, thalamic nuclei in the right hemisphere of brain LXXVIII (horizontal microscopic series) were located 2 mm more anterior as compared with the left side (sagittal series), which fact may be explained by difference in size and/or asymmetry. Spatial overlap between corresponding thalamic nuclei from the three series amounted to only 0–28% when superimposed in the ACPC reference space. Linear transformation towards an average led to significant increase (0–37%, $p < 0.001$) of the overlap and ameliorated the quality of the fit of thalamic borders. Limited increase of the overlap is in part due to pronounced differences in the size of thalamic nuclei between the series.

Keywords: Brain atlas; stereotaxy; thalamus.

On the Occasion of the 40th Anniversary of the Schaltenbrand and Bailey Stereotactic Atlas

Introduction

Since its first edition, which was published 40 years ago in 1959, the microscopic section of the Schaltenbrand stereotaxic atlas [1, 49–50] became a main reference for anatomical orientation in functional neurosurgery. At the time of this writing several digital implementations which support on-screen neurosurgical planning are available [32, 33, 38, 40, 53, 62, 63].

Accurate anatomical localization reduces operative time and thus the hazard of complications by minimizing the tissue volume to be explored physiologically [11, 21, 56]. Whereas the atlas is relevant for the choice of the trajectory, final identification of the target site relies on clinical observation of the semi-awake patient as well as electrophysiological feed-back [18, 30, 49, 52, 54] along the trajectory.

In the recent past, however, there have been reports on both pallidotomies and thalamotomies in which surgeons renounced any electrophysiological recordings [13, 15, 18, 42, 46, 65, 66]. The reasons were twofold: On the one hand, with the progress achieved in MR imaging [16, 26, 31] there has been a re-appraisal of the individual anatomical landmarks visualized in MR images for target localization [18, 31]. On the other hand, some centres perform functional radiosurgery [13, 15, 42, 46, 65, 66] in selected patients with the gamma knife, which implies lack of any electrophysiological verification. Thus the old questions as to how far thalamotomies and pallidotomies are anatomical or physiological operations and whether or not electrophysiological recordings along the trajectory are dispensable are again brought up for discussion.

Issues to be considered in this context do not only relate to the variability of the correlation between anatomy, somatotopography and modality content. Also, quantitative data as to the degree of anatomical

variability between individuals are needed. Such variability is already expressed in the atlas of Schaltenbrand and Wahren [1, 49, 50, 51] as three orthogonally sectioned microscopic series from two brain specimens are shown. Anatomically, loci with the same ACPC (anterior commissure–posterior commissure) co-ordinates in the sagittal, frontal, and horizontal series are therefore not exactly equivalent [10, 56]. For comparison of the position and size of structures between the three series, cumbersome and laborious measurements in the print atlas are of limited value. This is due to the lack of clearly identifiable anatomical landmarks within nuclear territories, uneven and coarse spacing between the slices [38], as well as the inclination of the horizontal slice series which was not sampled in the intercommissural ACPC reference system but sectioned parallel to Reid's plane [50, 51].

The goal of this study is to provide quantitative data on the geometrical relationships and the anatomical variability between the three microscopic series which allow comparison of target positions across the microscopic series. We felt that such study might also be helpful to understand problems encountered with the digital or non-digital registration of stereotaxic atlases to MR/CT images. Atlas-to-patient registration and the atlas-to-atlas registration of the three microscopic brainstem specimens of Schaltenbrand's atlas are closely related issues. Evaluation of the atlas-to-atlas registration, however, bears salient advantages in the operationalization of the problem: If to each voxel in the digital atlas an anatomical label is attached, strict evaluation criteria for the quality of the fit may be worked out. This applies especially to structures which are not visualized as such on current CT or MR images, e.g. the thalamic subdivisions.

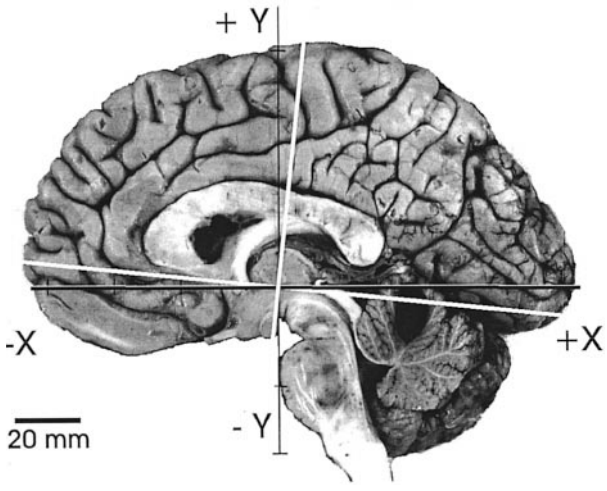

Fig. 1. Right hemisphere, intercommissural line (commissures connected centre to centre) and perpendicular through mid-intercommissural point indicated by black lines. In analogy to the Schaltenbrand and Wahren atlas [51] (Plate 50), white oblique indicates the dorsobasal zero plane of the horizontal histological series sampled in Reid's reference system. The angle between the horizontal ACPC plane and Reid's plane was 6° in the RH studied by Schaltenbrand and co-workers. Note that all structures sectioned by the plane indicated by white oblique have the dorsobasal ($Y_{hor\text{-}Reid^-}$) co-ordinates zero. Resampling of the horizontal digital slice series in the ACPC system thus implies a counterclockwise (*CCW*), mathematically positive rotation of the Reid co-ordinate axes (white) to the position of the ACPC coordinate axes (black)

Clinical Material and Methods

Analyses were carried out using three digitally interpolated voxel-based solid volume representations [38, 39]. Raw data stemmed from the microscopic part of the Schaltenbrand and Wahren (SW) atlas (2nd, 1977 edition [51]) in which three histological series are shown (frontal microscopic series, plates 23–29, right hemisphere (RH) of brain LXVIII; sagittal series, plates 34–49, left hemisphere (LH) of brain LXXVIII; horizontal series, plates 50–55, RH of the same brain). The frontal and sagittal series are orientated in the ACPC reference system. The horizontal series was (erroneously) sectioned parallel to Reid's plane which passes through the infraorbital margin of the orbital opening and the centre of the external acoustic meatus [1, 49, 50, 51].

Details concerning technical artefacts of the series and the algorithm used for 3-D interpolation have been described previously [38]. The three solid volume representations are isotropic (same resolution in X, Y, and Z) with a resolution of 0.25 mm/voxel. In the right hemisphere specimen from which the horizontal slice series of the Schaltenbrand and Wahren atlas was acquired, Reid's plane and the horizontal ACPC zero plane formed an angle of 6° so that the position of AC is more basal than the position of PC (see Plate 50 in Schaltenbrand's atlas [51] which indicates section planes of horizontal series and Fig. 1). Prior to comparison between atlases, we therefore resampled the Reid – orientated data from the horizontal series in the ACPC reference system, which implies a rotation of co-ordinate axes (anteroposterior (X) and dorsobasal (Y) axes) through an angle of 6° about a transverse axis (Z) with the midintercommissural point as centre (cf. Fig. 1, for details see Annex). In order to minimize integer rounding artefacts [47, 48] in the rotation, the resolution of all solid volumes was in the following set to 0.5 mm.

3-D Correspondence: Overlap Between Atlases

The correspondence of the 3-D position of anatomical structures between the three microscopic series was quantified by the calculation of their centres of gravity as well as the structurewise calculation of 3-D overlap. Using elementary formalism from the theory of sets, we defined three types of overlap which were quantified separately. For the casual reader, reference to Fig. 2 should be sufficient to grasp an intuitive notion of overlap types and the basic mathematical formalism below may be skipped.

If we consider an anatomical structure *str* (e.g. a thalamic division like V.im.e.), its spatial representation varies over the sagittal, frontal and horizontal digital atlases. We define the union of its atlas representations in 3-D as

$$V_{str} := V_{str,\,frontal} \cup V_{str,\,sagittal} \cup V_{str,\,horizontal}$$
$$:= \{V_{x,y,z} | V_{x,y,z} \in V_{str,\,frontal} \vee V_{x,y,z} \in V_{str,\,sagittal} \vee V_{x,y,z} \in V_{str,\,horizontal}\}$$

where $V_{x,y,z}$ are isotropic volume elements (voxels) and $V_{str,\,atlas}$ denotes the set of isotropic voxels in the solid volume occupied by the structure *str* under consideration. If there are no shared voxels of the structure under consideration there is no overlap: $V_{str,\,frontal} \cap V_{str,\,sagittal} \cap V_{str,\,horizontal} := \{\}$. If there is complete spatial correspondence between the three atlases the union of the sets is equivalent with their intersection:

$$V_{str} := V_{str,\,frontal} \cup V_{str,\,sagittal} \cup V_{str,\,horizontal}$$
$$:= V_{str,\,frontal} \cap V_{str,\,sagittal} \cap V_{str,\,horizontal}.$$

Variation between individuals, asymmetry of the hemispheres, technical flaws in the preparation of the atlases, different degrees of shrinkage, non-random distribution of section profiles and other artefacts, however, prevent complete overlap between atlases. For operational definition of the degree of correspondence between atlases, we define three types of overlap (Fig. 2): Overlap type 3 designates the set of voxels of a structure shared by all the three microscopic series. This is equivalent with the intersection of the three sets: $V_{str,\,overlap3} := V_{str,\,frontal} \cap V_{str,\,sagittal} \cap V_{str,\,horizontal}$ (black areas in Fig. 2) and the 'zone commune' of Guiot [20]. Overlap type 2 designates voxels at corresponding spatial postitions belonging to exactly two out of three atlases (hatched areas in Fig. 2):

$$V_{str,\,overlap_2} := \{((V_{str,\,frontal} \cap V_{str,\,sagittal}) \cup (V_{str,\,frontal} \cap V_{str,\,horizontal}) \cup (V_{str,\,sagittal} \cap V_{str,\,horizontal})) \backslash V_{str,\,overlap3}\}$$

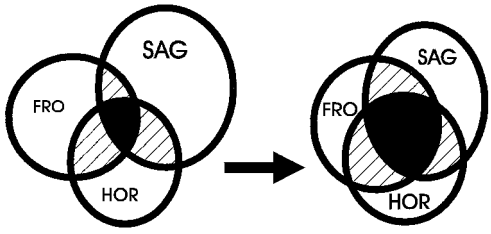

Fig. 2. Section profile of a structure in the frontal (FRO), sagittal (SAG), and horizontal (HOR) atlases. Black area indicates complete overlap of three atlases (overlap type 3, intersection) between atlases. Hatched areas designate areas in which two atlases overlap (type 2), empty areas within circles overlap type 1. V_{str} is the union of the atlas representations and corresponds to complete area covered by the three circles. Stereotactic normalisation (arrow) is assumed to equalise the size of structures and lead to an increase of overlap type 3 (black area). Note that only a 2-D slice is shown but evaluations were performed over complete 3-D extent of the structures

and overlap type 1 the set of voxels of a structure which belong to one and only one atlas $V_{str,\,overlap1} := V_{str} \backslash V_{str,\,overlap2}$ (empty fill areas in Fig. 2).

Averaging Based on Linear Regression Analysis

For the analysis of overlap between the sagittal, frontal and the horizontal (resampled in ACPC co-ordinate space) digital atlases we used a subset of 20 structures (cf. Table 1). It was considered mandatory that structures were precisely delineated and completely rep-

Table 1. *Centers of Gravity (COGs) of 21 Structures from Sagittal, Frontal and Horizontal (Resampled in ACPC) Schaltenbrand and Wahren [51] Atlas*

Nr	Structure	Mnemo	X_{sag}	X_{fro}	$X_{hor\text{-}acpc}$	Y_{sag}	Y_{fro}	$Y_{hor\text{-}acpc}$	Z_{sag}	Z_{fro}	Z_{hor}
1	Ncl. dorsomedialis	M.	7.3	7.5	4.8	7.8	8.0	7.6	6.0	4.6	5.8
2	Ncl. medialis fibrosus	M.fi	3.8	5.3	3.2	8.1	6.6	7.4	2.1	2.4	3.5
3	Ncl. medialis fasciculosus	M.fa.	6.5	6.4	2.8	7.2	8.3	8.3	6.4	5.6	6.4
4	Ncl. medialis caudalis	M.c.	11.4	11.2	9.1	8.7	10.8	7.5	8.0	6.2	7.7
5	Ncl. centralis	Ce.	9.4	9.2	7.2	3.0	3.1	3.1	10.2	7.8	9.2
6	Ncl. centralis parvocellularis	Ce.pc.	9.9	10.6	8.6	3.0	2.6	2.7	10.6	9.1	9.7
7	Ncl. centralis magnocellularis	Ce.mc.	7.8	8.5	6.4	3.2	3.6	3.4	8.9	7.1	8.9
8	Ncll. ventrales thalami	V..	5.9	7.1	4.1	3.2	4.5	2.0	13.5	12.2	12.5
9	Ncl. ventrocaudalis parvocellularis	V.c.pc.	10.7	8.7	8.0	0.5	−0.6	−1.3	15.7	9.9	13.0
10	Ncl. ventrocaudalis internus	V.c.i.	7.4	9.4	6.8	3.7	3.3	2.1	12.9	11.2	12.3
11	Ncl. ventrocaudalis externus	V.c.e.	10.8	11.7	8.1	4.3	4.7	1.9	17.3	15.9	17.1
12	Ncl. ventrointermedius internus	V.im.i.	3.7	5.1	2.3	4.8	5.5	2.8	10.9	10.1	10.8
13	Ncl. ventrointermedius externus	V.im.e.	6.9	5.7	3.2	4.4	5.2	2.2	16.6	13.0	14.3
14	Ncl. ventrooralis medialis	V.o.m.	1.7	1.5	1.7	0.3	0.3	1.2	5.0	4.1	5.5
15	Ncl. ventrooralis anterior	V.o.a.	0.1	−0.2	−2.6	3.7	4.2	3.5	11.4	9.3	11.0
16	Ncl. ventrooralis posterior	V.o.p.	2.6	3.0	0.7	4.1	4.2	2.2	12.4	12.0	11.4
17	Ncl. ventralis portae	V.por.	12.2	13.4	9.9	−0.4	4.4	−0.8	14.9	12.1	13.4
18	Ncl. ruber	Ru.	5.8	6.9	5.1	−7.1	−5.9	−5.1	5.1	4.7	5.3
19	Substantia nigra	Ni.	4.8	5.6	1.0	−10.1	−10.1	−8.1	10.0	8.1	10.1
20	Ncl. subthalamicus	S.th.	1.9	2.1	0.8	−3.8	−4.1	−1.5	12.0	9.5	12.7
21	Corpus mamillare	C.m.	−4.6	−4.3	−5.3	−9.3	−10.5	−8.1	2.4	2.1	2.5
	mean		6.0	6.4	4.1	10.1	1.9	2.3	8.4	1.6	9.7

Values are in mm relative to midintercomissural point (midpoint of ACPC line, centre of AC to centre of PC). Positive values for X are occipital, negative X is frontal, positive values for Y are dorsal, negative values basal, Z designates laterality (distance from midsagittal plane). See also Fig. 1. Values of the subthalamic nucleus from the horizontal series are approximated.

resented in each of the three microscopic series of the print atlas. Furthermore, we only selected structures approximately spherical or ellipsoid in shape. Thus centres of gravity (COGs) were expected to lie within structures indicating their anatomical site. Seventeen structures were thalamic, four extrathalamic (corpus mamillare, red nucleus, subthalamic nucleus, substantia nigra). Because of a digitization error in the horizontal series, the subthalamic nucleus had to be omitted from the analysis of overlap but its COG in the horizontal series (Table 1) could be sufficiently approximated. For each structure, the total number of voxels representing this structure in all the three atlas representations (V_{str}) was defined as 100% and the percentages of the overlap types ($V_{str,\,overlap1}$, $V_{str,\,overlap2}$, and $V_{str,\,overlap3}$) were calculated.

So as to obtain a measure for the location of the 21 structures in 3-D, we determined their centres of gravity in the three digital representations and performed linear regression analysis of their XYZ components. Note that COGs are thus regarded as anatomical landmarks and the problem to interactively define corresponding landmarks in the three series is evaded. Based on the regression equations, co-ordinates from one series may be transformed into anatomically correspondent co-ordinates of the other two series. Similarly, using the arithmetic mean of the centres of gravity from Table 1, regression equations which transform the three microscopic series into average size were determined the expectation being that the transform would increase spatial overlap of structures. This hypothesis was tested in the following by a second analysis of the overlap after transformation of the digital atlases towards an average (before correction vs after correction).

The necessary software was implemented by us in C++ under Unix on SUN workstations (Sun Microsystems, Inc., Palo Alto, CA) and uses OSF Motif (The Open Group, Menlo Park, CA) functionality. Statistical evaluations were carried out with the SAS software package (SAS Institute Inc., Cary, NC, software version V. 6.10). For linear regression analysis, we used the NOINT option in the MODEL statement of the GLM procedure. Thus any y-intercept ($y = a^*x + b$) is suppressed and a regression line ($y = a^*x$) through the origin (0/0) is forced. The slope (a) may thus be interpreted as scale factor along the axis under consideration. Intentionally, we do not use matrix notation here.

Results

Table 1 gives a survey of structures used for the analysis as well as the ACPC co-ordinates of their centres of gravity. COG-co-ordinates of the sagittal and frontal series were calculated from the untransformed digital atlases so that they are directly comparable with the print atlas. Anteroposterior X_{hor_acpc} and dorsobasal Y_{hor_acpc} co-ordinates refer to the horizontal digital atlases – after it had been resampled in the ACPC space – and must therefore be back-transformed (inverse transformation to Reid's space, see Annex) before they can be looked up in the print atlas. Note that the Z co-ordinate of the horizontal slices which indicates the distance from the midline (laterality) is not affected by the 6° rotation.

Pearson's correlation coefficients between the X, Y, and Z-co-ordinates of the corresponding 21 centres of gravity from the three atlases ranged between 0.944 and 0.976 ($\alpha < 0.0001$, not Bonferroni-corrected [45], Fig. 3). The latter finding indicates predominantly linear distortions in the microscopic series. The differences between the anteroposterior (X) co-ordinates of the sagittal and horizontal atlases as well as between the frontal and horizontal atlases were significant at the $p = 0.001$ level. There was also a significant difference in the laterality of structures between the sagittal and horizontal atlases on the one and the frontal atlas on the other hand ($p = 0.001$).

Tables 2 and 3 summarize the results obtained from linear regression analysis and list the equations needed to transform atlas co-ordinates. They may be used to identify the location of a target site after it has been selected in one series also in the other two (cf. annex).

For initial analysis of spatial overlap the three digital microscopic series were orientated and superimposed in the ACPC reference system. At this stage, type 3 overlap (cf. Fig. 4), ranged from 0% to 28% (mean for 20 structures: 8%), type 2 overlap from 8% to 37% (mean: 24%), and type 1 overlap from 44% to 92% (mean: 68%, Fig. 4).

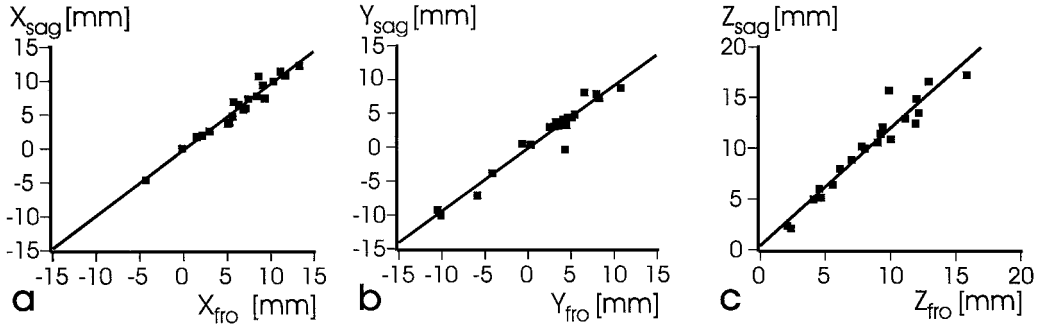

Fig. 3. Co-ordinates of centres of gravity (*COG*) calculated from frontal slice series vs. co-ordinates of centres of gravity from sagittal slice series. X designates the fronto-occipital ACPC axis, Y the dorsobasal axis, Z the transverse axis. The midintercommissural point is the origin of the co-ordinate system. Pearson's r-values were 0.976 (a), 0.963 (b), and 0.973 (c), respectively, $p < 0.0001$. COG values for subthalamic nucleus in horizontal series approximated

Table 2. *Regression Equations for Calculation of Co-Ordinates of Sagittal Slice Series from Frontal Slice Series and Vice Versa*

Eqn.	Parameter estimate	Standard error of parameter estimate	T for H0: parameter = 0	Prob > |T|
(2.1)	$X_{sag} = 0.949 * X_{fro}$	0.026	36.03	0.0001
(2.2)	$Y_{sag} = 0.906 * Y_{fro}$	0.046	19.72	0.0001
(2.3)	$Z_{sag} = 1.192 * Z_{fro}$	0.028	41.86	0.0001
(2.4)	$X_{fro} = 1.038 * X_{sag}$	0.029	36.03	0.0001
(2.5)	$Y_{fro} = 1.050 * Y_{sag}$	0.053	19.72	0.0001
(2.6)	$Z_{fro} = 0.829 * Z_{sag}$	0.020	41.86	0.0001

X Designates the fronto-occipital axis; *Y* the dorsobasal axis; *Z* the transverse axis. *Df* 1. Higher localization error in Y is in part due to analyzed nuclei which show only small variation of Y co-ordinates. Eqn. designates the different regression equations.

Table 3. *Regression Equations* ($df = 1$) *for Calculation of* X_{hor_acpc}, Y_{hor_acpc}, Z_{hor} *from Atlas Co-Ordinates of Frontal and Sagittal Atlases*

Eqn.	Parameter estimate	Standard error of parameter estimate	T for H0: parameter = 0	Prob > |T|
(3.1)	$X_{hor\_acpc} = 0.754 * X_{sag}$	0.038	19.66	0.0001
(3.2)	$Y_{hor\_acpc} = 0.827 * Y_{sag}$	0.044	18.72	0.0001
(3.3)	$Z_{hor} = 0.941 * Z_{sag}$	0.016	59.57	0.0001
(3.4)	$X_{hor\_acpc} = 0.718 * X_{fro}$	0.039	18.37	0.0001
(3.5)	$Y_{hor\_acpc} = 0.750 * Y_{fro}$	0.055	13.55	0.0001
(3.6)	$Z_{hor} = 1.126 * Z_{fro}$	0.024	47.43	0.0001

Note that rotation of co-ordinate axes of the horizontal digital atlas only affects X and Y but not the lateral co-ordinate Z (details see text and Annex).

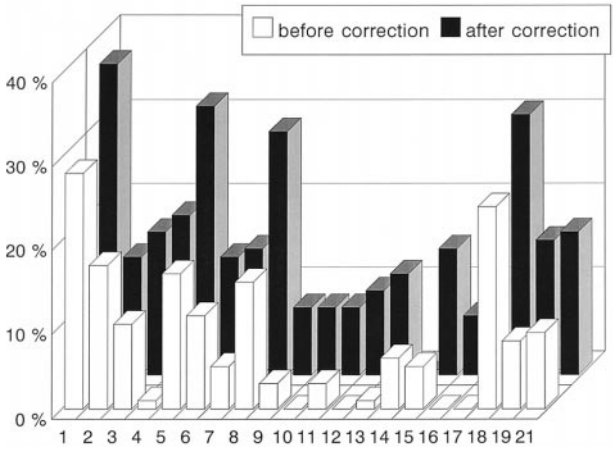

Fig. 4. Percentage of overlap type 3 in 20 structures before (hatched) and after (black) averaging the atlases for size, based on COG analysis and regression equations which transform all three atlases towards a grand average (details see Annex). Numbers refer to Table 1. In structures 10, 12, 16, and 17 the overlap was 0% before the correction

Averaging the three microscopic series for size based on the centres of gravity (cf. methods section) yielded the following results: The sagittal atlas co-ordinates had to be compressed in X, Y, and Z by 4 to 8% to meet the average. The frontal atlas was shrunk in anteroposterior (X) and vertical (Z) direction by 11%, its lateral co-ordinates (Y) were widened by 11%. The most pronounced changes were necessary for the rotated horizontal atlas in which the anteroposterior and the vertical co-ordinates had to be expanded by 19% and 15%, respectively. In the microscopic series averaged for size, again an analysis of the voxel overlap was carried out. After the transform (Fig. 4), type 3 overlap ranged from 0% to 37% (mean: 15%), type 2 overlap from 17% to 42% (mean 28%), and type 1 overlap from 37% to 83% (mean: 58%). The increase of overlap type 3 and the reduction of overlap 1 were significant at the $p = 0.0001$ level. From Fig. 5 and 6 reveals, that the correction towards an average also leads to better congruence of the thalamic contours – although the transform dislocates the commissures so that they no longer coincide.

The overall effect of averaging for size on the overlap of nuclei was less pronounced than we intuitively had expected. In the smallest out of 21 structures, the Ncl. ventro-oralis medialis (V.o.m., Fig. 7a), the overlap even deteriorated after spatial normalization (Fig. 4, structure 14).

Our definition of the percentage of overlap is dependent on the union of the volumes occupied by the structures in the three atlases V_{str} (Fig. 2). For purposes of control, we therefore determined nuclear vol-

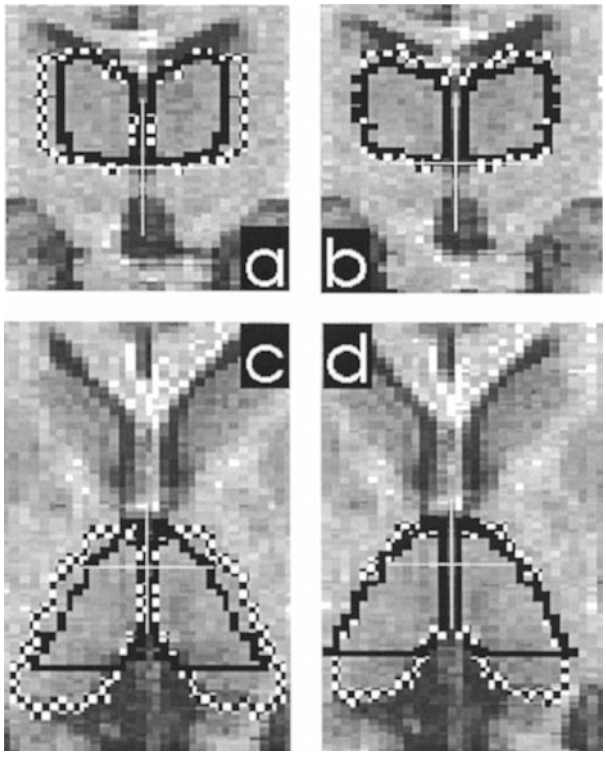

Fig. 5. Thalamic borders from sagittal (checkerboard) and frontal (black) digital series in superposition with MR images re-sliced parallel to ACPC. Frontal (a, b, 5 mm occipital to midintercommissural point) and horizontal (c, d, 6 mm dorsal to ACPC line) views. Frontal series does not cover pulvinar (black horizontal line in c and d gives occipital border of frontal series). Left column (a,c) before, right column (b,d) after spatial normalisation based on regression analysis of centres of gravity

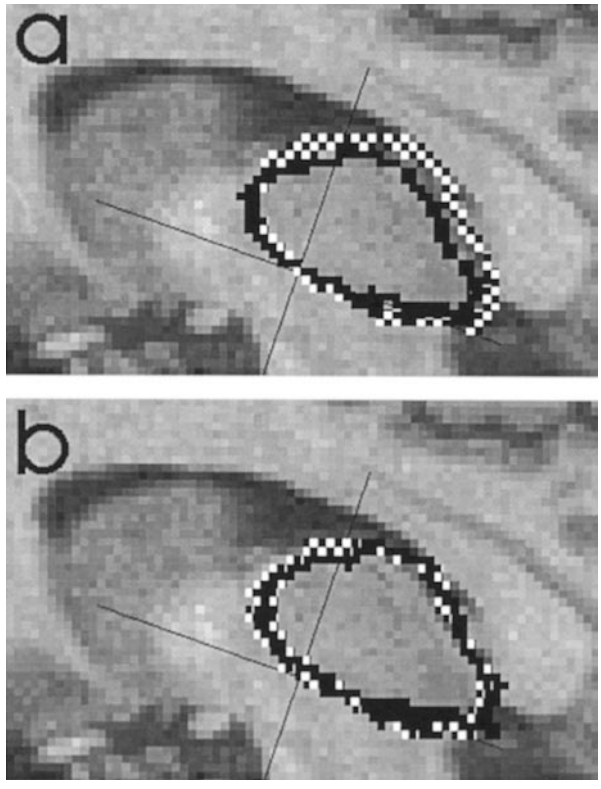

Fig. 6. Thalamic borders from sagittal (checkerboard) and horizontal (black) microscopic series rotated by 6° in superposition with sagittal MR image. Frontal is left. Top image before (a), bottom image (b) after spatial normalisation towards a grand average based on regression analysis of centres of gravity

umes for each microscopic series seperately. Results are shown in Fig. 7a–7c.

The volume of the subthalamic nucleus could not be exactly evaluated in the horizontal series due to a digitization error in 2 adjacent slices which became apparent after the interpolation. In the sagittal atlas, the volume of S.th. was 267 mm^3, in the frontal atlas 156 mm^3.

As additional reference, the volumes enclosed by the thalamic contours were calculated. The volume of the sagittally sectioned thalamus amounts to 7.75 cm^3, the volume of the horizontally sectioned thalamus is 5.50 cm^3 resulting in a volume ratio sagittal/horizontal of 1.41. The volume of the frontally sectioned thalamus was assessed at 5.12 cm^3. As occipital parts of the pulvinar are lacking in the frontal microscopic series (Fig. 5c and d, cf. methods section), however, the latter figure must be corrected. If we assume that 1/4 of its volume is not covered (Fig. 5c), the true volume of the frontally sectioned thalamus would be 6.83 cm^3 and the volume ratio sagittal/frontal equal 1.13.

Data are in good accord with Table 3, Eqns. 3.1–3.3, which indicates an approximate volumetric proportion of $1/(0.75 * 0.83 * 0.94) = 1.71$ between the sagittally and the horizontally sectioned thalami if the thalamus is considered an ellipsoid. As volumetric proportion of the sagittal vs frontal series, 1.03–1.10 is expected (calculated from Table 2; Eqns. 2.1–2.3, $0.95 * 0.91 * 1.19 = 1.03$; from Table 2, Eqns. 2.4–2.6: $1/(1.04 * 1.05 * 0.83) = 1.10$).

Discussion

The phenomenon that the same ACPC co-ordinates describe different anatomical loci in the three microscopic series of the SW atlas is not unknown [10, 56]. Our approach quantifies the differences and gives exact parameters for the mappings of the three digital series into each other under the constraint that transforms

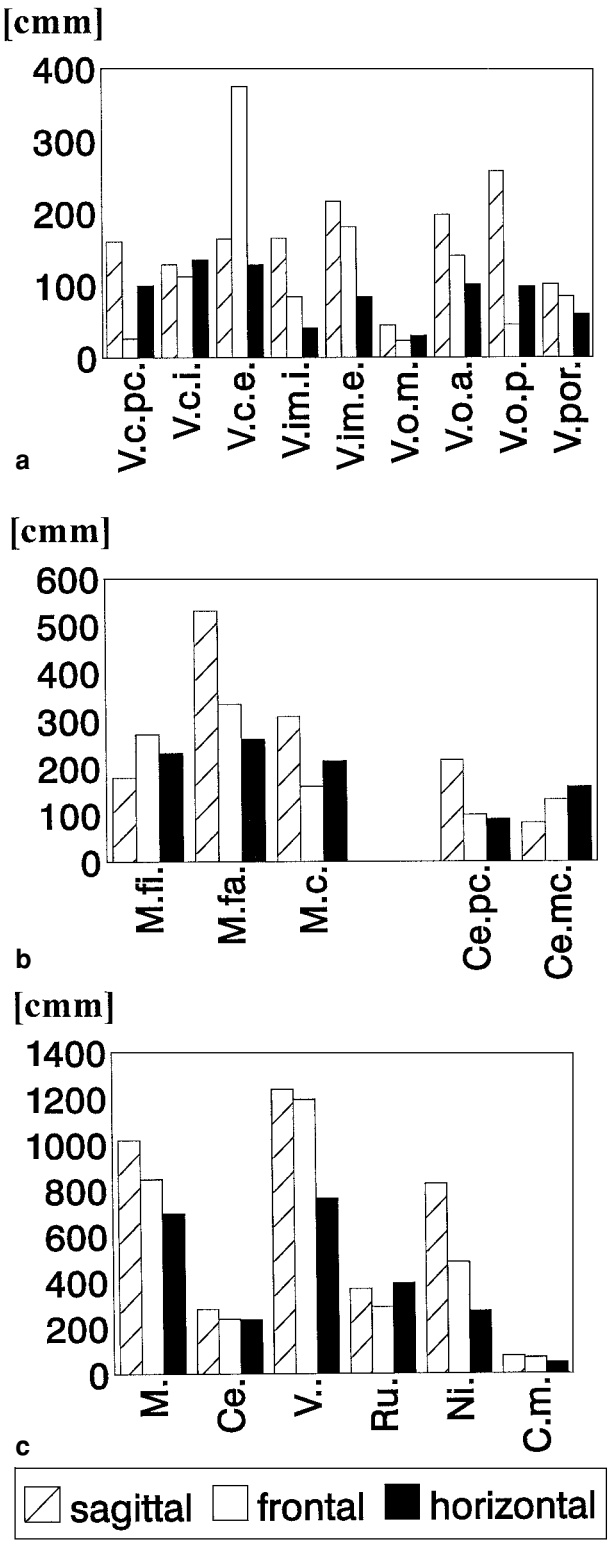

Fig. 7. Volumes of nine ventral tier nuclei of lateral nuclear mass (a) and selected subnuclei of nucleus medialis dorsalis (M.) and nucleus centralis thalami (Ce.) (b). Volumes of nuclei from Fig. 5 summed up to V.. and of nuclei from Fig. 6 summed up to M. and Ce. are shown in (c). Mnemos cf. Table1. Note the stronger relative variations of volumes in frontal series (a)

are linear. It allows for the calculation of anatomically corresponding (target-) co-ordinates, comparison of the positions of nuclei between series (Table 1), as well as transformations of the complete series into each other (Tables 2 and 3). Establishing these relationships is moreover helpful for digital registration of the three microscopic series to the patient's images, for implementation of linked cursor movements in the three series, and for the recording of physiological data in a stereotaxic data base [19, 61, 64], as only the parameters for the transform of one of the atlas spaces into the patient's image space have to be determined.

Limitations of Approach

The approach is limited by the selection criteria for the 21 structures and the realm of the regression equations is possibly restricted to their immediate vicinity. Note that distortion between series is considered linear [36, 55]. The analysis focuses on the close neighbourhood of surgically important thalamic and subthalamic targets. The pulvinar, which provides relevant parts of the thalamic borders, had to be excluded from comparison as its occipital parts are not covered by the frontal microseries [51] (Fig. 5c and 5d). In the horizontal series, the substantia nigra is to a smaller part not shown so that data (Table 1, Ni. in Fig. 7c) must be interpreted with care. The pallidum was not included in the digitization. Volumetric results may be burdened with artefacts of the interpolation procedure which might cause stronger variation in the volumes of smaller structures. However the amount of interpolation artefacts is low, compared with irregularities in the microscopic definitions of borders [38].

Analysis of Centres of Gravity

The co-ordinates of the centres of gravity give an estimate of structure location in 3-D and indicate in which nuclei the deviations between the three microscopic series are pronounced (Table 1). Due to 3-D interpolation co-ordinates could be calculated in a spatial continuum thus avoiding discretization by the uneven and coarse sampling intervals of the histological slices in the print atlas [38, 51].

Our data indicate that the frontal series has to be widened by 19% in lateral (Z) direction so as to match it to the sagittal series (error term 3%, Table 2 (Equation 2.3), Fig. 5). This somewhat exceeds values reported by Bertrand [10] who on the basis of trial and

error widened the coronal sections by 13% in both lateral and anteroposterior directions. Along the a.p. axis, however, we assume that not stretching by 13% but instead compression of the X co-ordinates by 4–5% is mandatory (Table 2, Eqn. 2.1).

By resampling of the digitized horizontal microscopic series (plates 50–55 [51]) in the intercommissural reference space, not only its lateral (Z) co-ordinates but also the anteroposterior (X) and vertical (Y) co-ordinates may be compared with the sagittal and frontal microscopic series. Our data confirm that there is good correspondence in the laterality structures between the sagittal and the horizontal, but not with the frontal series (see Y values in Table 3).

Asymmetry and position of nuclei. Table 1 reveals, that the centres of gravity in the right hemisphere of brain LXXVIII (horizontal slice series) are on average 2 mm more frontal (smaller X-co-ordinates) than in the left hemisphere of the same brain (sagittal series). This finding cannot only be attribuated to the smaller size of the right thalamus of brain LXXVIII since the difference still turned out significant after scaling of the anterior-posterior co-ordinates of the horizontal atlas by 19% ($p < 0.0002$). Thus it might result from both shrinkage and asymmetry between the thalami of either side. It is well known that the anterior portion of the right hemisphere and the posterior portion of the left hemisphere extend farther than their counterparts, particularly in right-handers [35]. As the thalamus is concentrically connected with cortical areas and wiring is kept to a minimum, the asymmetry of the hemispheres should have an impact on the a.p. location of thalamic nuclei. Although, van Buren and Maccubbin [60] who measured 60 sites in 58 comparisons did not detect that differences between the right and left hemispheres had any effect on measurements of the sites. Details on what exactly has been measured are not reported [60]. In contrast, early CT studies indicate that the thalamus and the calcified glomus of the choroid plexus of the lateral ventricles lie posterior to their counterparts in the same hemisphere that extends further posteriorly [35]. Recently, evidence for positional left-right asymmetry of the fornix, a structure closely related to the thalamus, has been reported by Supprian and Hoffmann [57]. In horizontal magnetic resonance images the left columna fornicis was predominantly (60.3%) caudal to the right whereas the inverse was only observed in 13%. Positional differences were markedly demonstrated near the anterior nuclear group of the thalamus [57].

Volumes of Thalamic and Adjacent Nuclei

The pronounced differences between the volumes of the nuclei in the three microscopic series (Fig. 7) should be interpreted with care as measured volumes depend on a combination of factors: Variability between individuals, asymmetry of nuclear volumes between the two hemispheres, different degrees of tissue shrinkage, potential error in the digital interpolation and the morphological classifications of the authors. Differences in weight and dimensions of the brains (LXVIII, 1470 gr, 172 mm length, 138 mm width; LXXVIII: 1400 gr, 170 mm length, 135 mm width [1]) as well as in the length of the intercommissural line (LXVIII 22 mm, LXXVIII 23 mm [1] are, however, neglegible. Both the brain specimens stem from male individuals aged 51 and 40 years who died from tuberculosis of the lungs [1]. The sagittally sectioned thalamus has the greatest volume of all the three specimens (7.75 cm^3) and this volume comes close to data in the living recently published by Collins, Kabani, and Evans [12]. Using an automatic hybrid segmentation scheme they determined gross cerebral structure volumes in MRI data sets of 152 normal subjects. Values for the thalamus were (mean $\pm$ standard deviation) 8.3 ± 0.9 cm^3 on the right and 9.0 ± 1.0 cm^3 on the left side [12].

Volumes of the subthalamic nucleus reported by Collins and co-workers are, however, lower (0.1 ± 0.0 cm^3 on the right, and 0.1 ± 0.0 cm^3 on the left side [12]) than in our study (see result section) which might result from classification problems in the image segmentation because of the fibre content of S.th. and its direct vicinity. Lange, Thorner, and Hopf [34] reported on the size of the subthalamic nucleus in 12 normal brains. The mean fresh volume amounted to 144 mm^3 in males and to 134 mm^3 in females. Kandel [30] (p. 14) quotes a study of Bedrensky and Vasin [9] in which the length of the subthalamic nucleus varies from 7 to 11 mm (average 8 mm) , the width from 8 to 14 mm (average 9 mm) and the height from 4 to 8 mm (average 6.5 mm). From the reported average data, using a formula popular in the estimation of lesion size [15] one would expect a volume of the subthalamic nucleus of $= \frac{4\pi}{3} * \left(\frac{8+9+6.5}{6}\right)^3 mm^3 = 252$ mm^3,

and, taking the minima and maxima reported by Bedrensky and Vasin [9], a range from 133 mm^3 to 697 mm^3.

Volume asymmetry. Eidelberg and Galaburda were the first to report asymmetry of thalamic nuclear volumes in humans. They demonstrated significant left sided bias of the lateralis posterior nucleus but were not able to detect any side difference of the CM/Pf complex and the nuclei of the pulvinar [14]. For hodological reasons they concluded that interhemispheric volume differences should occur with nuclei related to asymmetric areas of the human cortex but not in the so-called specific and intralaminar nuclei [14].

Expected volume pattern. Following these assumptions, the specific and intralaminar nuclei in the Schaltenbrand and Wahren atlas should mirror the volume ratios of the thalami, at least with regard to the sagittal and horizontal series which stem from the same brain but might have been subject to different degrees of shrinkage. Strong deviations from the thalamic volume ratio sagittal/horizontal (≈ 1.41–1.71) or sagittal/frontal (≈ 1.03–1.13) and the 'normal' volume pattern ($V_{str,sagittal} > V_{str,frontal} > V_{str,horizontal}$) may thus indicate variability between individuals, asymmetry, artefacts of the interpolation, or histological misclassification in the print atlas.

Ventral tier of lateral nuclear group. Table 4 and Fig. 7a reveal that the ventral tier nuclei of the RH of brain LXXVIII (horizontal series) are smaller than those of the LH (sagittal series). If volumes of the nine nuclei in Fig. 7a are summed up to V.. (Fig. 7c), the volume ratio is 1.62 (Table 5) in favour of the left side. Pitfalls in the histological classification of subnuclei are indicated by extreme deviations from this ratio (Table 4, Fig. 7a, e.g. V.c.p.c., V.c.e., V.o.p.). Earlier analysis revealed, that the technical quality of the frontal series is superior to the other two [38]. As volumetric analysis indicates (Fig. 7a), histological parcellations in the frontal series are, however, more noisy, i.e. deviating from the 'normal' volume pattern, than in the other two series. In the frontal series, e.g., V.c.e. covers a volume of 375 mm^3, in the sagittal atlas of only 164 mm^3. V.c.e. furthermore undergoes unnaturally abrupt changes at its anterior and posterior borders (SW atlas, frontal plates 28 and 29). This may besides variability be due to the fact that many thalamic nuclei have a roughly transverse boundary. Therefore they are much easier to delineate in the sagittal or horizontal plane [59].

Volumes are comparable to data from Armstrong who sums up V.c.i, V.c.e., V.im.i. and V.im.e. to the ventrobasal complex [3]. In two histologically processed human brains, Armstrong reported a volume of the ventrobasal complex of 273 and 300 mm^3. From the SW atlas we determined volumes of 674 mm^3 (sagittal series), 752 mm^3 (frontal series), and 388 mm^3 (horizontal series), respectively.

Table 4. *Volumes of Nuclei of Ventral Tier of Lateral Nuclear Group in Sagittal* (V_{sag}), *Frontal* (V_{fro}), *and Horizontal* (V_{hor}) *Digital Microscopic Series*

Mnemo	V_{sag} [cmm]	V_{fro} [cmm]	V_{hor} [cmm]	V_{sag}/V_{fro}	V_{sag}/V_{hor}
V.c.pc.	161	26	99	6.19	1.63
V.c.i.	129	112	135	1.15	0.96
V.c.e.	164	375	128	0.44	1.28
V.im.i.	165	84	41	1.96	4.08
V.im.e.	216	181	84	1.20	2.57
V.o.m.	45	23	30	1.96	1.50
V.o.a.	197	140	101	1.40	1.96
V.o.p.	258	45	98	5.73	2.63
V.por.	101	85	60	1.20	1.68

From the data, which are graphed in Fig. 7a, volume ratios were calculated. Mnemonic codes from Table 1. Note that sagittal (*LH*) and horizontal (*RH*) series were taken from the same brain specimen.

N. centralis. The parvocellular part of the N. centralis (Ce.pc.) occupies about two thirds of its volume [59]. This proportion has only been worked out in the sagittal series (Fig. 7b). Note that the morphological distinction beetween the magnocellular and parvocellular parts of the nucleus is not very clear [6, 59] whereas differentiation of the magnocellular division and the adjacent parfascicular nucleus relies on more distinct staining of the slender, multipolar or triangular cells of the latter complex [43, 59]. We assume that the borders betwen of the magno- and parvocellular parts of Ce. were not consistently classified in the three series (Fig. 7b). If Ce. pc. and Ce. mc. are summed up to Ce. (Fig. 7c), the volume ratio between the right and left hemispheres of brain LXXVIII equals 1.2 (Table 5). The volume of Ce. in the sagittal series is 282 mm^3. Hopf [27] whose values must be halved for comparison [4, 27] assessed the volume of the Cm-Pf complex in fresh brain specimens at $720/2 = 360$ mm^3.

Table 5. *Volume Ratios of Larger Nuclear Territories in Sagittal* (V_{sag}), *Frontal* (V_{fro}), *and Horizontal* (V_{hor}) *Digital Microscopic Series. Mnemonic Codes from Table 1*

Mnemo	V_{sag} [cmm]	V_{fro} [cmm]	V_{hor} [cmm]	V_{sag}/V_{fro}	V_{sag}/V_{hor}
M.	1018	847	697	1.20	1.46
Ce.	282	237	235	1.19	1.20
V..	1238	1194	764	1.04	1.62
Ru.	369	290	393	1.27	0.94
C.m.	77	68	47	1.13	1.62
Mean				1.17	1.37

N. dorsomedialis. The dorsomedial nucleus (M., Fig. 7c) is largest in the sagittal, followed by the frontal and the horizontal series. However, there is marked variation of the volume pattern of its subnuclei (Fig. 7a) which might indicate error in the definition of the compartments. The medial, magnocellular part is equivalent to M.fi., the lateral, parvocellular part to M. fa.. Some authorities claim that the pronounced variation of these compartments in size is caused by differences in staining intensity, not real size [5]. Van Buren and Borke were unable to replicate the subdivision of the mediodorsal complex into a magnocellular and a parvocellular part on the basis of measurements of the diameter of cells [59]. On the other hand it is argued that the pars parvicellularis (M. fa. [5]), forms the largest component [6, 17] in newer species which was again clearly worked out in the sagittal series of the SW atlas only (Fig. 7b).

Contrary to the specific nuclei, in the case of the dorsomedial nucleus we cannot rule out the possibility that it is asymmetric as it is connected to asymmetric regions of the cerebral cortex [17, 22]. Pakkenberg [44], however, in a neurostereological study was unable to detect significant differences between the volumes of the dorsomedial nuclei of either side. In 11 normal controls, the mean volume of M.. was 411 mm^3 with a broad variation from $\approx$300–650 mm^3. In the interpolated Schaltenbrand data (Fig. 7c) volumes are 1018 mm^3 in the sagittal, 847 mm^3 in the frontal, and 697 mm^3 in the horizontal series. Hopf [27] determined a volume of $2030/2 = 1015$ mm^3 in fresh brain specimens.

Granularity of Histological Classification vs Intra-Rater Reliability

If volumes of the smaller nuclei (Fig. 7a and 7b) are summed up to larger nuclear territories (Fig. 7c), potential error in the intricate nuclear parcellations should become less and volume proportions between the three thalami more influential on the results. Consequently it reveals that the larger subdivisons of the thalamus are greatest in the sagittal, followed by the frontal, then by the horizontal atlas ($V_{str,\,sagittal} > V_{str,\,frontal} > V_{str,\,horizontal}$) and volume ratios show less variation (cf. Table 4 vs Table 5). In some smaller structures which are characteristic in their appearance and thus easily identified in the histological sections independent of the section plane, this 'normal' volume pattern is also expressed (e.g. in the Ncl. ventralis portae, V. por, Fig. 7a and Table 4 or in the Corpus mamillare, C.m., Fig. 7c and Table 5). Similar to the lateral geniculate [6], the volume of the C.m. may be regarded as control for shrinkage (77 mm^3 in the sagittal, 68 mm^3 in the frontal and 47 mm^3 in the horizontal series, volume ratios in Table 5). The volumes of the red nucleus (Ru., see Table 5 and Fig. 7c) are strikingly similar in the three series (369 mm^3 in the sagittal, 290 mm^3 in the frontal and 393 mm^3 in the horizontal series). This might indicate less differences in shrinkage in the brainstem and/or a greater degree of reliability in the classification of C.m. and Ru.. With reference to Kandel [30] (p. 15) who quotes a study of Yukharev [67] on the average dimensions of the red nucleus, and again using the formula reported by Friehs *et al.* [15] an average volume of the Ru.. of $= \frac{4\pi}{3} * \left(\frac{9.2 + 7.7 + 7.6}{6}\right)^3 mm^3 = 284$ mm^3 is expected. Note that identification of the nucleus in the frontal plane is impeded by dentatothalamic and dentatorubral fibres which might account for the smaller value in the frontal series.

Volumetry of thalamic nuclei from the SW atlas reveals that their classification based on fuzzy, verbally conveyed cytoarchitectonic criteria [22, 23] is probably insufficient. The high granularity of the subdivisions of thalamic nuclear compartments in the SW atlas is at variance with the obvious differences of their volumes in the three microscopic series. It explains in part why 3-D overlap between the same nuclei from the three microscopic series is apparently poor even after COG based stereotaxic spatial normalization which leads to a good fit of thalamic borders (Figs. 5 and 6). Note that there was even disagreement on nuclear subdivisions between Hassler and Schaltenbrand [23]. Hassler distinguishes 121 different thalamic nuclei, Olszewski 50 subdivisions in the thalamus of the Old World Monkey, Jones discerns 54 structures [8,

28, 43]. As histological classifications are not only dependent on fuzzy morphological characteristics but also on the form and size of the nuclei and their geometrical relationships to the section plane some error is unevitable. Van Buren worked out the importance of objective morphometric criteria like histograms of the soma diameter of cells and had difficulties in confirming many of Hassler's divisions. Furthermore, he stressed potential hazards and pitfalls of the definition of nuclear borders in the frontal plane [59].

This study demonstrates the need for additional objectivation of thalamic subdivisions for establishing stereotaxic atlases, e.g. by multiarchitectonic classification [7, 24, 25, 28, 29, 37, 41, 59] also in the human [37] and studies into the anatomical variability in (left vs right hemisphere [14]) and between individuals [2].

Although it indicates potential pitfalls of mere anatomical target localization it demonstrates ways to reconcile data from different sources. Solid volume representation of stereotaxic data enables straightforward and structured analysis of their intra- and inter-individual variability [2, 37, 43, 59, 60], analysis of their consistency and mutual relationships, and also covers aspects of the quality control of the histological raw data [38].

An interesting aspect for further study is the possible computer simulation of linear stereotaxic normalization procedures and their effects on the internal congruence of thalamic subdivisions from different brain specimens (cf. early work from Brierley and Beck [11], Guiot [20], van Buren and Maccubin [60], procedures described in this paper). This includes closer analysis of the question whether surface matching of thalamic borders, ACPC based matching, or local matching which mainly relies on the position of one of the commissures only is preferable with regard to a specific target [11, 37, 60]. In this context it is worthwhile mentioning the 'prinicple of vicinity' proposed already by Talairach *et al.* [58] and van Buren and Maccubin [59, 60] which in essence says that the more distant structures are from a landmark the higher is the variability. This would imply that reference structures close to a target have the highest relevance for its localization, so that e.g. structures situated very close to PC should predominantly be related to PC (and not AC or the midintercommissural point) as landmark.

Furthermore, the computer may selectively display a weighted melange from different atlas data bases: the centres of gravity from all three series, areas and types of overlap between different series as well as other available atlases, eventually in conjunction with probability maps or fuzzy weighting components [39], together with the patient's images. Such approaches have already been implemented in our software routines and replace the static iconic representation of one individual anatomy in a stereotaxic atlas by a dynamic variability profile which may nevertheless be tailored to the individual anatomy of the patient.

Annex

The analysis described in this paper has several steps. It uses the fully digital, voxel based, interpolated volume representation of the data [38]. As in the print atlas, the digital horizontal slice series [51] was first registered in Reid's reference system, and these co-ordinates are designated as $\mathbf{X}_{\text{hor\_Reid}}$, $\mathbf{Y}_{\text{hor\_Reid}}$, and $\mathbf{Z}_{\text{hor}}$. Then, based on the individual angulation (6°) of the intercommissural plane and Reid's plane in the specimen studied by Schaltenbrand (see plate 50 [51] and also Fig. 1) the horizontal digital atlas was re-sampled in the ACPC co-ordinate system which implies a transformation of co-ordinates (rotation of coordinate axes). The resulting co-ordinates are designated as $\mathbf{X}_{\text{hor\_acpc}}$, $\mathbf{Y}_{\text{hor\_acpc}}$ and $\mathbf{Z}_{\text{hor}}$. Note that the transform from Reid's space to the ACPC space has no effect on the $\mathbf{Z}_{\text{hor}}$ co-ordinates, i.e. the laterality of structures.

Generally speaking, rotation of co-ordinate axes is one in which a pair of axes giving the co-ordinates of a point (x, y) are rotated through an angle φ resulting in a new pair of axes in which the point has co-ordinates (x', y'). The transformation equations are trigonometric in form:

$$\mathbf{x}' = \mathbf{x}\cos\varphi + \mathbf{y}\sin\varphi, \quad \text{and}$$
$$\mathbf{y}' = -\mathbf{x}\sin\varphi + \mathbf{y}\cos\varphi$$

Example 1. Assessing the Effect of the Rotation of Co-ordinate Axes on Points Located on Reid's Line

The effect of the transformation is obvious if we consider a point on Reid's zero plane (e.g. on the white line in Fig. 1) near the frontal pole of the brain at a distance of $X_{\text{hor\_Reid}} = -70$ mm from the midintercommissural point. Hence, as $Y_{\text{hor\_Reid}}$ equals zero

$$\mathbf{X}_{\text{hor\_acpc}} = \mathbf{X}_{\text{hor\_Reid}} * \mathbf{\cos 6^\circ} \approx \mathbf{-70\,mm} * \mathbf{0.99452}$$
$$\approx \mathbf{-69.62\,mm}, \quad \text{and}$$
$$\mathbf{Y}_{\text{hor\_acpc}} = -\mathbf{X}_{\text{hor\_Reid}} * \mathbf{\sin 6^\circ} \approx -(\mathbf{-70\,mm}) * \mathbf{0.10453} \approx \mathbf{7.32\,mm}.$$

If we consider a corresponding point on the white line but near the occipital pole ($X_{\text{hor\_Reid}} = 70$ mm, $Y_{\text{hor\_Reid}} = 0$ mm) it will be attributated the ACPC co-ordinates:

$$\mathbf{X}_{\text{hor\_acpc}} = \mathbf{X}_{\text{hor\_Reid}} * \mathbf{\cos 6^\circ}$$
$$\approx \mathbf{70\,mm} * \mathbf{0.99452} \approx \mathbf{69.62\,mm}, \quad \text{and}$$
$$\mathbf{Y}_{\text{hor\_acpc}} = -\mathbf{X}_{\text{hor\_Reid}} * \mathbf{\sin 6^\circ} \approx \mathbf{-70\,mm} * \mathbf{0.10453} \approx \mathbf{-7.32\,mm}.$$

This renders evident also from Fig. 1: The more anterior a point is located on the white line indicating Reid's zero plane (i.e. with negative $X_{\text{hor\_Reid}}$-co-ordinates and $Y_{\text{hor\_Reid}} = 0$ mm) the more its Y-co-ordinate has to be incremented if the same point is transformed to $Y_{\text{hor\_acpc}}$. The more posterior a point is located on the white line indicating Reid's zero plane (i.e. with positive $X_{\text{hor\_Reid}}$ co-ordinates and $Y_{\text{hor\_Reid}} = 0$ mm) the more its Y-co-ordinate has to be decre-

mented if the same point is registered in the ACPC- co-ordinate system. Note that the effect of the transform on the X-co-ordinates, because of cos 6° ≈ 0.99452 is minimal, whereas displacement of the Y-co-ordinates substantially increases with the anteroposterior (X) distance from the midintercommissural point. Hence the greater the absolute value of the X-coordinate of a point, the more pronounced is the difference of its dorsobasal (Y) co-ordinate between the horizontal and the frontal/sagittal atlases already for geometrical reasons – leaving differences in size and shape between the three thalamic specimens out of consideration.

Calculation of centres of gravity. In the digital, voxel based representation, each anatomical structure is represented under a different code. Structures may therefore be individually addressed and handled seperately so that for each of the 21 structures the individual centre of gravity could be determined. Centres of gravity were calculated after the formulae:

$$\overline{x_{str}} = \frac{1}{M_{str}} \iiint_{(K_{str})} x\rho(x,y,z)\,dx\,dy\,dz,$$

$$\overline{y_{str}} = \frac{1}{M_{str}} \iiint_{(K_{str})} y\rho(x,y,z)\,dx\,dy\,dz, \quad \text{and}$$

$$\overline{z_{str}} = \frac{1}{M_{str}} \iiint_{(K_{str})} z\rho(x,y,z)\,dx\,dy\,dz \text{ with } M_{str} \text{ being the mass of the}$$

structure under consideration, K_{str} the spatial region covered by the structure and assuming a homogeneous density for all structures of $\rho(x,y,z) = 1$.

Linear regression analysis was performed for the three axes (X = anteroposterior, Y = dorsobasal, Z = transverse axis) separately. The regression equations allow for easy transformation of target co-ordinates from the three microscopic series into each other. Suppression of the y-intercept in the regression equations allows for easy interpretation of the slope as scale factor and also for the interpretation of the error terms given in Tables 2 and 3.

Analysis of overlap. Based on the data from Table 1 for each of the 21 structures the arithmetic means of the COGs over the three series $(X_{sag} + X_{fro} + X_{hor\_acpc})/3$, $(Y_{sag}, + Y_{fro} + Y_{hor\_acpc})/3$, and $(Z_{sag} + Z_{fro} + Z_{hor})/3$ were calculated. Then regression equations which transform the sagittal, frontal and ACPC-orientated horizontal atlas to these average co-ordinates were calculated and used to transform the three digital atlases towards "average" size. The effect of averaging on the overlap of structures is shown in Fig. 4 ("before correction" vs. "after (size) correction"). The regression equations themselves are not supplied, as the focus in this paper is on those regression equations (table 2 and 3) which transform the co-ordinates of the sagittal, frontal, and horizontal series into each other.

Use of regression equations. For a better understanding of the train of thought of the regression analysis, note that Fig. 3 graphs regression equations 2.1-2.3 from Table 2 and that the data in Fig. 3 stem from the respective columns in Table 1. Generally speaking, the regression equations (Tables 2 and 3) mirror the linear component of the deformation between the three specimens analyzed by Schaltenbrand and co-workers. By assessing these linear relationships in quantitative terms we do not exclude possible localized or global non-linear distortion which is in part expressed by the error terms in Table 2 and 3. For the transformation of frontal and sagittal atlas co-ordinates into each other, the regression equations from Table 2 suffice, as both series were sampled in the ACPC reference system:

Example 2. Defining the Anatomically Correspondent Point in the Frontal Series from a Target Defined in the Sagittal Series

We select a point P_{sag} within V.im.e. in the sagittal series, Plate 46 ($Z_{sag} = 16$ mm lateral to the midplane) with the co-ordinates $X_{sag} = 6$ mm occipital to the midintercommissural point, $Y_{sag} = 4.75$ mm dorsal to the ACPC line. Thus the point is defined approximately in the centre of the sagittal section profile of V.im.e. in this slice. Note that Plate 46 contains the largest section profile of V.im.e. in the sagittal series. If one would rely on the fact that the same ACPC co-ordinates describe the same anatomical loci in the three microscopic series, P_{sag} would be (erroneously) located within the Ncl. reticularis of the thalamus of the frontal series (cf. plate 28, F.p 7.00 mm), i.e. too lateral.

Based on the linear regression equations (2.4)–(2.6) from Table 2 we find the following approximation for P_{fro} in the frontal series:

$$\mathbf{X_{fro} = 1.038 * X_{sag} = 1.038 * 6.00\,mm = 6.23\,mm},$$

$$\mathbf{Y_{fro} = 1.050 * Y_{sag} = 1.050 * 4.75\,mm = 4.99\,mm},$$

$$\mathbf{Z_{fro} = 0.829 * Z_{sag} = 0.829 * 16.00\,mm = 13.27\,mm}.$$

The anatomically corresponding geometrical locus of P_{sag} (as defined in the sagittal slice series of the print atlas) in the frontal series is therefore in plate 28, F.p 7.00 mm (≈ 6.23), 13.3 mm lateral to the midline and 5 mm dorsal to the ACPC line. Note that the correction mainly has an effect on the laterality (Z-coordinate) as after the COG analysis, the frontal slice series of the Schaltenbrand and Wahren atlas is substantially smaller than the sagittal one in lateral direction (cf. Fig. 5, a and c).

Example 3. Defining the Anatomically Correspondent Point in the Horizontal Series from a Target Defined in the Sagittal Series

What is the anatomical correspondence of the same point P_{sag} ($X_{sag} = 6.00$ mm, $Y_{sag} = 4.75$ mm, $Z_{sag} = 16.00$ mm) in the horizontal series? The COG analysis was performed after the rotation of co-ordinate axes, i.e.after resampling the horizontal digital atlas in the ACPC reference system. In a first step we therefore have to transform the co-ordinates from the sagittal series into co-ordinates of the horizontal digital atlas sampled in the ACPC reference system using equations (3.1)–(3.3) from Table 3:

$$\mathbf{X_{hor\_acpc} = 0.754 * X_{sag} = 0.754 * 6.00\,mm = 4.52\,mm}$$

$$\mathbf{Y_{hor\_acpc} = 0.827 * Y_{sag} = 0.827 * 4.75\,mm = 3.98\,mm}$$

$$\mathbf{Z_{hor} = 0.941 * Z_{sag} = 0.941 * 16.00\,mm = 15.06\,mm}.$$

Note that X_{hor_acpc}, Y_{hor_acpc}, and Z_{hor} correspond to the digital horizontal atlas registered in the ACPC reference system. Hence these co-ordinates are not directly comparable with the print atlas. So as to obtain the exact site of P_{sag} in the horizontal series from the print atlas, the X and Y co-ordinates, must be back-transformed from the ACPC into Reid's co-ordinate system which implies back-rotation (inverse transformation) of the co-ordinate axes (X and Y) about the Z-axis by -6 degrees with the midintercommissural point as origin. With an angle $\varphi(-6°)$ the "transforms" are:

$$\mathbf{X_{hor\_Reid} = X_{hor\_acpc} * \cos(-6°) + Y_{hor\_acpc} * \sin(-6°)}$$

$$\mathbf{\approx 4.52 * 0.994522 + 3.98 * -0.10453\,mm \approx 4.91\,mm}$$

$$\mathbf{Y_{hor\_Reid} = -X_{hor\_acpc} * \sin(-6°) + Y_{hor\_acpc} * \cos(-6°)}$$

$$\mathbf{\approx -4.52 * -0.10453 + 3.98 * 0.99452\,mm \approx 4.43\,mm}.$$

The point P_{sag} with the co-ordinates $X_{sag} = 6$ mm, $Y_{sag} = 4.75$, $Z_{sag} = 16$ mm, in the sagittal atlas therefore corresponds to $X_{hor\_Reid} \approx 4.91$ mm, $Y_{hor\_Reid} \approx 4.43$ mm, $Z_{hor} \approx 15.06$ mm in the horizontal atlas plates (Plate 52, H.d + 4.0).

References

1. Amador LV, Blundell JE, Wahren W (1959) Description of co-ordinates of the deep structures. In: Schaltenbrand G, Bailey P (eds) Introduction to stereotaxis with an atlas of the human brain, vol I. Thieme, Stuttgart, pp 16–28
2. Andrew J, Watkins ES (1969) A stereotaxic atlas of the human thalamus and adjacent structures. A variability study. Williams & Wilkins, Baltimore
3. Armstrong E (1979) A quantitative comparison of the hominoid thalamus. I. Specific sensory relay nuclei. Am J Phys Anthrop 51: 365–382
4. Armstrong E (1980) A quantitative comparison of the hominoid thalamus. II.Limbic nuclei anterior principalis and lateralis dorsalis. Am J Phys Anthrop 52: 43–54
5. Armstrong E (1990) Limbic thalamus: anterior and mediodorsal nuclei. In: Paxinos G (ed) The human nervous system. Academic Press, San Diego London, pp 469–481
6. Armstrong E, Frost GT (1988) The diencephalon. A comparative review. In: Schwartz JH (ed) Orang-utan biology. Oxford University Press, New York, pp 177–188
7. Asanuma C, Thach WT, Jones EG (1983) Cytoarchitectonic delineation of the ventral lateral thalamic region in the monkey. Brain Res Rev 5: 219–235
8. Axer H, Niemann K (1994) Terminology of the thalamus and its representation in a part-whole relation. Method Inform Med 33: 488–95
9. Bedrensky LA, Vasin NY (1981) The anterior cerebral commissure as a stereotaxic guiding point. Vopr Neirokhir 4: 30–34 (Russian)
10. Bertrand G (1982) Computers in stereotaxic surgery. In: Schaltenbrand G, Walker AE (eds) Stereotaxy of the human brain. Thieme, Stuttgart, New York, pp 364–371
11. Brierley JB, Beck E (1959) The significance in human stereotaxic brain surgery of individual variation in the diencephalon and globus pallidus. J Neurolog Neurosurg Psychiatry 22: 287–298
12. Collins DL, Kabani NJ, Evans AC (1998) Automatic volume estimation of gross cerebral structures. Proc. 4th. International Conference on Functional Mapping of the Human Brain. Neuroimage 7(4): S702
13. Duma CM, Jacques DB, Kopyov OV, Mark RJ, Copcutt B, Farokhi HK (1998) Gamma knife radiosurgery for thalamotomy in parkinsonian tremor: a five-year experience. J Neurosurg 88: 1044–1049
14. Eidelberg D, Galaburda AM (1982) Symmetry and asymmetry in the human posterior thalamus. I. Cytoarchitectonic analysis in normal persons. Arch Neurol 39: 325–332
15. Friehs GM, Norén G, Ohye C, Duma CM, Marks R, Plombon J, Young RF (1996) Lesion size following gamma knife treatment for functional disorders. Stereotact Funct Neurosurg [Suppl] 1(66): 320–328
16. Fujii Y, Nakayama N, Nakada T (1998) High-resolution T_2-reversed magnetic resonance imaging on a high magnetic field system. J Neurosurg 89: 492–495
17. Fuster JM (1989) The prefrontal cortex. Anatomy, physiology and neuropsychology of the frontal lobe, 2nd edn. Raven Press, New York
18. Giller CA, Dewey RB, Ginsburg MI, Mendelsohn DB, Berk AM (1998) Stereotactic pallidotomy and thalamotomy using individual variations of anatomic landmarks for localization. Neurosurgery 42: 56–65
19. Giorgi C, Cerchiari U (1991) Contemporary stereotaxic atlasses: Merging of functional data with individual morphological MRI acquisitions. Acta Neurochir [Suppl] (Wien) 52: 69–71
20. Guiot G, Brion S, Akerman M (1961) Anatomie stéréotaxique du pallidum interne du thalamus et de la capsule interne. Étude des variations individuelles. Ann Chir 15: 557–586
21. Hariz MI (1997) Image-guided functional ablation of the brain. In: Salles AAF, Lufkin RB (eds) Minimally invasive therapy of the brain. Thieme, New York, Stuttgart, pp 142–156
22. Hassler R (1959) Anatomy of the thalamus. In: Schaltenbrand G, Bailey P (eds) Introduction to stereotaxis with an atlas of the human brain, vol I. Thieme, Stuttgart, pp 230–290
23. Hassler R (1982) Architectonic organization of the thalamic nuclei. In: Schaltenbrand G, Walker AE (eds) Stereotaxy of the human brain. Thieme, Stuttgart, New York, pp 140–180
24. Hirai T, Jones EG (1989) A new parcellation of the human thalamus on the basis of histochemical staining. Brain Res Rev 14: 1–34
25. Hirai T, Jones EG (1993) Comparative anatomical study of ventrolateral thalamic mass in humans and monkeys. Stereotact Funct Neurosurg 60: 6–16
26. Holmes CJ, Hoge R, Collins L, Woods R, Toga AW, Evans AC (1998) Enhancement of MR images using registration for signal averaging. J Comput Assist Tomogr 22: 324–333
27. Hopf A (1965) Volumetrische Untersuchungen zur vergleichenden Anatomie des Thalmus. J Hirnforsch 8: 25–38
28. Jones EG (1985) The thalamus. Plenum Press, New York
29. Jones EG (1990) Correlation and revised nomenclature of ventral nuclei in the thalamus of human and monkey. Stereotact Funct Neurosurg 54: 1–20
30. Kandel EI (1989) Functional and stereotaxic neurosurgery. Translated from Russian by George Watts, translation edited by A. Earl Walker. Plenum Publishing Corporation, New York
31. Kawashima Y, Chen HJ, Takahashi A, Hirato M, Ohye C (1992) Application of magnetic resonance imaging in functional stereotaxic thalamotomy for the evaluation of individual variations of the thalamus. Stereotact Funct Neurosurg 58: 33–38
32. Kazarnovskaya MI, Borodkin SM, Shabalov VA, Krivosheina VY, Golanov AV (1991) 3-D computer model of subcortical structures of human brain. Comput Biol Med 21: 451–457
33. Kimura M, Otsuki T (1993) Reconstruction of a 3-D stereotaxic brain atlas and its contour-to-contour elastic deformation. SPIE Image Capture, Formatting and Display 1897: 60–68
34. Lange H, Thorner G, Hopf A (1976) Morphometric-statistical structure analysis of human striatum, pallidum and nucleus subthalamicus. IIII. Nucleus subthalamicus. J Hirnforsch 17: 31–41
35. LeMay M (1984) Radiological, developmental, and fossil asymmetries. In: Geschwind N, Galaburda Am (eds) Cerebral dominance. The biological foundations. Harvard University Press, Cambridge, pp 26–52
36. Minoshima S, Koeppe RA, Frey KA, Kuhl DE (1994) Anatomic standardization: Linear scaling and nonlinear warping of functional brain images. J Nuclear Med 35: 1528–1537
37. Morel A, Magnin M, Jeanmonod D (1997) Multiarchitectonic and stereotaxic atlas of the human thalamus. J Comp Neurol 387: 588–630
38. Niemann K, Naujokat C, Pohl G, Wollner C, Keyserlingk DGv (1994) Verification of the Schaltenbrand and Wahren stereotaxic atlas. Acta Neurochir (Wien) 129: 72–81

39. Niemann K, van Nieuwenhofen I, Berks G, von Keyserlingk DG (1996) The Schaltenbrand and Wahren stereotaxic atlas: conflicts in a histological database resolved by fuzzy set representation. Proc. 4th European congress on Intelligent Techniques and Soft Computing (EUFIT 96). Mainz-Verlag, Aachen, pp 2117–2122
40. Nowinski WL, Fang A, Nguyen BT, Raphel JK, Jagannathan L, Raghavan R, Bryan RN, Miller GA (1997) Multiple brain atlas database and atlas-based neuroimaging system. Comp Aided Surg 2: 42–66
41. Ohye C (1990) Thalamus. In: Paxinos G (ed) The human nervous system. Academic Press, San Diego London, pp 439–468
42. Ohye C, Shibazaki T, Hirato M, Inoue H, Andou Y (1996) Gamma thalamotomy for Parkinsonian and other kinds of tremor. Stereotact Funct Neurosurg [Suppl] 1(66): 333–342
43. Olszewski J (1952) The thalamus of the macaca mulatta. An atlas for use with the stereotaxic instrument. Karger, Basel, New York
44. Pakkenberg B (1992) The volume of the mediodorsal thalamic nucleus in treated and untreated schizophrenics. Schizophr Res 7: 95–100
45. Perneger TV (1998) What's wrong with Bonferroni adjustments. Brit Med J 316: 1236–1238
46. Rand RW, Jacques DB, Melbye RW, Copcutt BG, Fisher MR, Levenick MN (1993) Gamma knife thalamotomy and pallidotomy in patients with movement disorders: preliminary results. Stereo Funct Neurosurg [Suppl] 1(61): 65–92
47. Rogers DF, Adams JA (1976) Mathematical elements for computer graphics. McGraw-Hill, New York
48. Rosenfeld A, Kak AC (1982) Digital Picture Processing. Computer Science and applied mathematics, vol 2. 2nd edn. Academic Press, San Diego
49. Schaltenbrand G, Bailey P (1959) Introduction to stereotaxis with an atlas of the human brain, vols I–III. Thieme, Stuttgart
50. Schaltenbrand G, Wahren W (1959) The plates. In: Schaltenbrand G, Bailey P (eds) Introduction to stereotaxis with an atlas of the human brain, vol I. Thieme, Stuttgart, pp 9–15
51. Schaltenbrand G, Wahren W (1977) Atlas for stereotaxy of the human brain. 2nd edn. Thieme, Stuttgart
52. Schaltenbrand G, Walker AE (eds) (1982) Stereotaxy of the human brain. Anatomical, physiological and clinical applications, 2nd edn. Thieme, Stuttgart, New York
53. Serra L, Nowinski WL, Poston T, Hern N, Meng LC, Guan CG, Pillay PK (1996/7) The brain bench: virtual tools for stereotaxic frame neurosurgery. Med Image Anal 1: 317–329
54. Shima F, Morioka T, Tobimatsu S, Kavaklis O, Kato M, Fukui M (1991) Localization of stereotaxic targets by microrecording of thalamic somatosensory evoked potentials. Neurosurgery 28: 223–230
55. Sorlié C, Bertrand O, Yvert B, Fromen JC, Pernier J (1997) Matching of digitised brain atlas to magnetic resonance images. Med Biol Eng Comput 35: 239–245
56. Spiegelmann R, Friedman WA (1991) Rapid determination of thalamic CT-stereotaxic coordinates: a method. Acta Neurochir (Wien) 110: 77–81
57. Supprian Z, Hofmann, E (1997) The fornix of the human brain: evidence of left/right asymmetry on axial MRI scans. Surg Radiol Anat 19: 105–109
58. Talairach J, David M, Tournoux P, Corredor H, Kvasina T (1957) Atlas d'anatomie Stéréotaxique. Réperage radiologique indirect des noyaux gris centrau, des régions méséncephalo-sous-optique et hypothalamique de l'homme. Masson & Cie, Paris
59. Van Buren JM, Borke RC (1972) Variations and connections of the human thalamus, vols 1 + 2. Springer, Berlin Heidelberg New York
60. Van Buren JM, Maccubbin DA (1962) An outline atlas of the human basal ganglia with estimation of anatomical variants. J Neurosurg 19: 811–839
61. Vitek JL, Bakay RAE, Hashimoto T, Kaneoke Y, Mewes K, Zhang JY, Rye D, Starr P, Baron M, Turner R, DeLong MR (1998) Microelectrode-guided pallidotomy: technical approach and its application in medically intractable Parkinson's disease. J Neurosurg 88: 1027–1043
62. Williams ML (1997) Graphics Workstations for Therapy of the Brain. In: Salles AAF, Lufkin RB (eds) Minimally invasive therapy of the brain. Thieme, New York, Stuttgart, pp 17–30
63. Yeo TT, Nowinski WL (1997) Functional neurosurgery aided by use of an electronic brain atlas. Acta Neurochir [Suppl] (Wien) 68: 93–99
64. Yoshida M (1993) Three-dimensional electrophysiological atlas created by computer mapping of clinical responses elicited on stimulation of human subcortical structures. Stereotact Funct Neurosurg 60: 127–134
65. Young RF, Vermeulen SS, Grimm P, Posewitz A (1996) Electrophysiological target localization is not required for the treatment of functional disorders. Stereotact Funct Neurosurg [Suppl] 1(66): 309–319
66. Young RF (1997) Functional disease of the brain: treatment by gamma knife radiosurgery. In: Salles AAF, Lufkin RB (eds) Minimally invasive therapy of the brain. Thieme, New York, Stuttgart, pp 225–234
67. Yukharev SP (1979) Neurosurgical anatomy of Forel's H-field as applied to campotomy. Vopr Neirokhir 2: 48–52 (Russian)

Comments

This is an excellent paper analyzing the known discrepancies between the three oriented planes of the SW atlas on which is based the current opinion that atlases are basically wrong. The didactic explanation of their COG based method makes it understandable to the reader how they did proceed.

They provide a table of transformation between frontal, sagittal and horizontal coordinates and the COG coordinates in these 3 planes for 21 nuclei. They also use their measurements to substantiate right to left asymmetry.

Although these data do not demonstrate any unknown fact, they are useful to the stereotactitian reader

A. L. Benabid

In this very laborious work the authors quantify what we already knew and what can be expected from a topographic atlas based on sections of different brain specimens. Namely that there are significant interindividual variations in brains. To know the existence of this problem is crucial for functional neurosurgery, to know its extent is useful. And this information is given by the authors in the current article.

The topic of this article is highly specialized given the fact that it is focused on a book of which less then 2000 have been printed and sold.

For those who are familiar with the atlas and/or interested in functional neurosurgery it would be worth to read it.

F. Alesch

Correspondence: Klaus Niemann, M.D., Department of Neuroanatomy, RWTH (Rheinisch-Westfälische Technische Hochschule) Aachen, Wendlingweg 2, D-52074 Aachen, Germany.